LETTER Communicated by Bard Ermentrout

Type I and Type II Neuron Models Are Selectively Driven by Differential Stimulus Features

Germán Mato
matog@cab.cnea.gov.ar
Inés Samengo
samengo@cab.cnea.gov.ar
Comisión Nacional de Energía Atómica and Consejo Nacional de Investigaciones Científicas y Técnicas, Centro Atómico Bariloche and Instituto Balseiro, 8400 San Carlos de Bariloche, R.N., Argentina

Neurons in the nervous system exhibit an outstanding variety of morphological and physiological properties. However, close to threshold, this remarkable richness may be grouped succinctly into two basic types of excitability, often referred to as type I and type II. The dynamical traits of these two neuron types have been extensively characterized. It would be interesting, however, to understand the information-processing consequences of their dynamical properties. To that end, here we determine the differences between the stimulus features inducing firing in type I and type II neurons. We work with both realistic conductance-based models and minimal normal forms. We conclude that type I neurons fire in response to scale-free depolarizing stimuli. Type II neurons, instead, are most efficiently driven by input stimuli containing both depolarizing and hyperpolarizing phases, with significant power in the frequency band corresponding to the intrinsic frequencies of the cell.

1 Introduction

Several research lines have recently used reverse correlation methods to determine the stimulus features that are most relevant in shaping the probability to generate spikes of sensory neurons. Just to mention a few examples, in the visual system, Fairhall et al. (2006) revealed multiple spatiotemporal receptive fields (STRF) driving salamander retinal ganglion cells. In turn, Rust, Schwartz, Movshon, and Simoncelli (2005) explored the STRF of macaque V1. In the somatosensory system, Maravall, Petersen, Fairhall, Arabzadeh, and Diamond (2007) employed covariance analysis to disclose the effect of adaptation on the shift of coding properties in rat barrel cortex.

Here, we are interested in exploring the way the relevant stimulus features driving neuronal firing depend on the intrinsic dynamical properties of the cell. To that end, we work with a time-dependent stimulus representing the total input current arriving at the axon hillock. In any real

system, this input current may enter into the cell in several ways. For example, it can pass through receptor channels, activated by specific physical agents (light, sound, or temperature, for example) relevant to a particular sensory modality. Alternatively, it may be the integrated synaptic current entering a central cell through its numerous dendrites or through an intracellular electrode. In any case, we shall assume that our time-dependent stimulus $s(t)$ represents an ionic current that, after propagating all along the spatial extension of the neuron, arrives at the axon hillock, where the decision to fire or not to fire is taken. Hence, we shall be dealing only with the temporal, and not spatial, properties of the input current.

Our aim is to understand the relation between the stimulus attributes that most strongly affect the firing probability and the intrinsic dynamical properties of the neurons. This line of research was initiated with the study of the relevant stimulus features driving integrate-and-fire model neurons (Agüera y Arcas & Fairhall, 2003) and in Hodgkin-Huxley cells (Agüera y Arcas, Fairhall, & Bialek 2003). Later Hong, Agüera y Arcas, and Fairhall (2007) explored a broader class of neuron models, determining the effect of several dynamical features on the relevant stimulus dimensions. Here, we extend those analyses, searching for unifying properties that characterize the way in which the type of bifurcation at firing onset affects stimulus selectivity and information transmission. We therefore compare the relevant stimulus features driving two broad classes of neuron models: type I and type II dynamics. The distinction between type I and type II excitability was first introduced by Hodgkin (1948) when studying the dependence of the firing rate of a neuron with the injected current. Later, more detailed classifications of neuronal excitability were introduced (Ermentrout, 1996; Izhikevich, 2007), in terms of the bifurcation type at firing onset. In all cases, type I cells undergo a saddle node bifurcation on the invariant circle, at threshold. Type II neurons instead may correspond to three different bifurcations: a subcritical Hopf bifurcation, a supercritical Hopf bifurcation, or a saddle node bifurcation outside the invariant circle. Most of type II conductance-based Hodgkin-Huxley-type neuron models, however, undergo a subcritical Hopf bifurcation. Therefore, when exploring type II neuron models here, we focus on those exhibiting a subcritical-Hopf bifurcation.

When type I neurons are stimulated by a constant input current, the onset of firing is brought about by a saddle node bifurcation (Izhikevich, 2007). In the upper panel of Figure 1, a schematic representation of the topology of a type I bifurcations is depicted. For subthreshold input currents, Figure 1A, the system contains two orbits forming a closed figure, connecting two fixed points: one of them is stable, and the other is unstable. As the injected current I increases, the two fixed points come nearer each other, so that when I reaches a critical value I_c, the two points coalesce into a single one (see Figure 1B). Thereafter, both equilibrium points disappear, and the system moves in a periodic orbit (see Figure 1C).

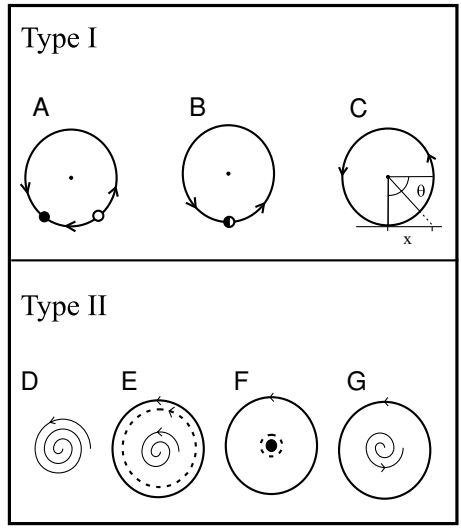

Figure 1: Schematic representation of the bifurcation underlying the onset of firing in type I (A, B, C) and type II (D, E, F, G) neuronal models. The input current is increased from left to right, and in both cases, the system passes from a single fixed point (A and D) describing the subthreshold rest state to a firing limit cycle (C and G).

The topological properties of the subcritical Hopf bifurcation (also called inverted Hopf bifurcation) characteristic of many type II models are shown in the lower panel of Figure 1. For subthreshold input currents, there is only a single stable spiral fixed point, Figure 1D. As the current increases, there is a region far away from the fixed point where the radial velocity diminishes. At a certain critical current I_g, two closed orbits appear through a global bifurcation—the outermost stable and the inner one unstable (see Figure 1E). As the current is increased further, the unstable limit cycle shrinks, approaching the spiral fixed point, Figure 1F. When I reaches a second critical value I_c, the unstable orbit coalesces onto the fixed point. If I grows beyond I_c, the fixed point is turned into an unstable spiral node, and the only stable attractor of the system is the distant limit cycle, Figure 1G.

These two types of cells differ from each other in the bifurcation underlying the onset of firing. This comprises a clear topological difference that endows each type with specific dynamical properties. It would be interesting, however, to be able to identify the functional consequences of these dynamical differences. More precisely, we would like to determine in which way the two neuron types differ regarding their information-processing properties. Specifically, what kind of time-dependent stimulus is needed to induce spiking in a type I neuron, and how does this stimulus differ

from the one needed to excite a type II neuron? To answer this question, we explore the relevant stimulus features shaping the firing probability of type I and type II neurons by means of covariance analysis. In the first place, we work with conductance-based models, capturing the biophysically relevant processes. We then compare the results obtained for these realistic models with those derived from reduced neural models, which minimally describe the essential dynamical features of both neuronal types. We conclude that close to threshold, the relevant stimulus features driving a given cell are determined by the type of bifurcation.

2 The Models and Their Phase-Resetting Curves

In the case of type I neurons, we use the model neurons introduced by Wang and Buzsaki (1996) to describe hippocampal interneurons. This model (hereafter called WB), when stimulated with a suprathreshold constant input current, settles into a limit cycle, embedded in its three-dimensional phase space. As the input current is lowered, the firing frequency tends to zero, and the system displays a saddle node bifurcation into its resting state. Therefore, the WB model can be classified as type I. The detailed equations are displayed in appendix A. The second model is the original Hodgkin-Huxley (HH) neuron (see the equations in appendix B). This is a four-dimensional system that, at threshold, undergoes a subcritical Hopf bifurcation and is therefore classified as type II.

Figure 1 shows the qualitative behavior of type I and type II neural models in response to constant stimulation. We see that both systems oscillate periodically if the input is above the critical current I_c. The behavior of these systems when weakly perturbed by rapid current injections is characterized by the phase-response function $Z(t)$. This function describes how the phase of a spike is advanced or delayed, depending on the time t at which the system is perturbed (Kuramoto, 2003). More precisely, $Z(t)$ is defined as the ratio between the change of the phase and the size of the perturbation in the limit of small perturbations. In principle, the perturbation can be applied along any of the variables of the dynamical system, giving rise to a multidimensional phase-response function. In this letter, however, perturbations are always instantiated only as input currents, thereby affecting only a single direction in phase space: the one parallel to the membrane potential axis V. Hence, here, $Z(t)$ represents the magnitude of a phase-response function always pointing in the direction of V (or $-V$, if $Z(t)$ is negative). By convention, we stipulate that the time of spike generation (defined as the point where the voltage crosses the value 0 mV from below) corresponds to $t = 0$. The function $Z(t)$ has the same period T as the firing cycle of the neuron, which in turn depends on the size of the constant input current.

In Figures 2A and 2B, the phase-response curve of the WB and HH models is depicted. The most salient difference between the two models is that $Z(t)$ is (almost) always positive for the WB model, whereas it exhibits both

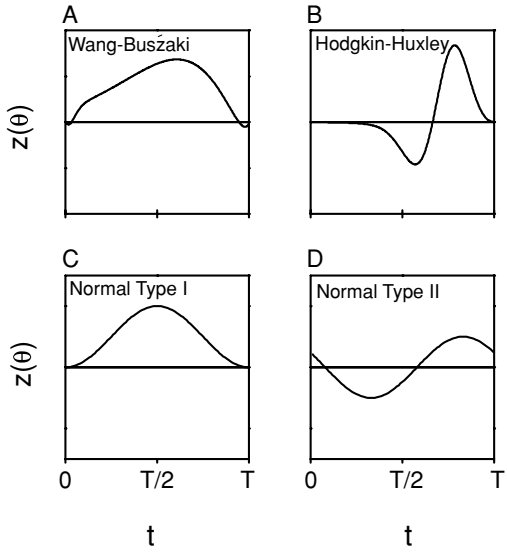

Figure 2: Type I (left panels) and type II (right panels) phase response curves. The realistic models (WB and HH) are shown in the upper row, and the simplified normal forms are depicted in the bottom row.

positive and negative regions in the HH case (Hansel, Mato, & Meunier, 1995). Hence, a small depolarizing perturbation always results in anticipated firing in the WB model, whereas it may either advance or delay spiking in the HH model, depending on when exactly the perturbation is delivered. Both the WB and HH models show maximal sensitivity to the external perturbation far away from the spiking events. In addition, the HH model shows more evidently that right after the spike ($t \approx 0$), the system is rather unresponsive to incoming perturbations due to refractoriness.

In the upper panels of Figure 2, the DC component of the input current was fixed to a different value in each model so as to obtain a firing rate of 62.5 Hz in both cases (that is, $T = 16$ ms). When the DC input current is lowered, the HH model eventually enters in its bistable region at a finite firing frequency. The WB model instead can be driven with arbitrarily low firing rates. Actually, as the firing rate of the WB model is diminished, the small region of negative $Z(t)$ that is observed for $t \approx T$ and $t \approx 0$ disappears, leaving a purely positive phase-resetting curve. In fact, only near threshold do type I neurons display a purely positive phase resetting; if the input current increases, the curve begins to resemble that of type II neurons.

Near threshold, hence, the HH neuron shows a phase-resetting curve that is qualitatively different from that of the WB neuron. The question now arises whether this difference is specific to these two neuron models, or

whether it is always found when comparing a type I with a type II cell. We therefore analyze the phase-resetting curves of the reduced models. To that end, the input current is written as

$$I = I_c + \epsilon^2 i. \tag{2.1}$$

Ermentrout and Kopell (1986) and Ermentrout (1996) have shown that the dynamics of any type I neuron can be reduced to a one-dimensional equation for a variable x that represents the projection of the state of the system on the direction of phase space that loses stability at threshold. After a nonlinear transformation $x = \tan(\theta/2)$ and rescaling the temporal variable, this dynamics can be written as

$$\frac{d\theta}{dt} = [1 - \cos(\theta)] + \alpha\,[1 + \cos\theta]\,, \tag{2.2}$$

where $\alpha = \eta/2\epsilon q$ plays the role of a bifurcation parameter. It is defined in terms of q (depending solely on the dynamical properties of the original model) and η (proportional to the magnitude of the perturbation i). Both parameters may be derived from the equations of the full-blown system. Spike generation is associated with $\theta = \pm\pi$ (see Figure 1). Notice that equation 2.2 is valid for any neural model sufficiently close to a saddle node bifurcation. Hence, regardless of the diversity of dynamical richness, near firing onset, the whole collection of type I conductance-based models is topologically equivalent to a system controlled by just a single parameter α.

For one-dimensional systems, the phase-response curve can be evaluated analytically (Hansel et al., 1995; Kuramoto, 2003). For this case, it is found that

$$Z(t) \propto \sin^2(\pi t/T)\,, \tag{2.3}$$

as depicted in Figure 2C. Notice that as in the WB model, $Z(t)$ is always positive, with maximum sensitivity near $t = T/2$. Therefore, up to some positive scaling constant, the response function of type I models near the bifurcation is universal. In what follows, all numerical integrations of the reduced (or normal) type I system are carried out with equation 2.2.

Why is the phase-response function always positive for type I neurons, and why does it approach zero in the vicinity of spiking times? Near the bifurcation, type I neurons spend most of their time in the neighborhood of $\theta = 0$ or $x = 0$ (that is, far from the spiking region $\theta = \pi$ or $x \to \pm\infty$). The slow dynamics near $\theta = 0$ is a footprint of the two fixed points that appear through a saddle node bifurcation, when the input current is lowered below the critical value. As a consequence, in the slightly suprathreshold regime,

the system spends a large fraction of each period around $x = 0 = \theta$. Hence, almost all the perturbations find the system in this region, where positive perturbations advance the phase of the neuron. Therefore, for almost all t, external perturbations result in anticipated spike generation and, thereby, in a positive phase-response curve. In addition, in the vicinity of $\theta = \pm\pi$, the system sets into the rapid acceleration associated with spike generation. In this region, the dynamics is dominated by the catalytic opening of voltage-dependent conductances, not by the detailed temporal properties of the perturbing current. Hence, $Z(t) \to 0$, when $t \approx T$.

We now turn to the reduced model of the HH neuron. In this case, the onset of firing is governed by a subcritical Hopf bifurcation. Only two of the four eigenvalues lose stability at threshold, meaning that the bifurcation takes place in two dimensions. Hence, the reduced model is two-dimensional, and similar to Brown, Moehlis, and Holmes (2004), we choose to analyze it in polar coordinates,

$$\frac{\mathrm{d}r}{\mathrm{d}t} = \alpha r + cr^3 + fr^5 \tag{2.4}$$

$$\frac{\mathrm{d}\phi}{\mathrm{d}t} = 2\pi(\beta + dr^2 + gr^4), \tag{2.5}$$

where, for subcritical bifurcations, $c > 0$, $f < 0$. Notice that the reduced system described by equations 2.4 and 2.5 represents a combination of two bifurcations: a nonlocal saddle node bifurcation of limit cycles far away from the fixed point (represented in Figure 1E) and a local subcritical Hopf bifurcation (see Figure 1F). This means that the parameters defining the spatially extended system 2.4 and 2.5 cannot be obtained by a local reduction of the full-blown model. Therefore, they have to be understood as an approximate representation of the original system, with its same topological properties.

The bifurcation parameter α is proportional to $I - I_c$. When $\alpha > 0$, the fixed point $r = 0$ is unstable, and all trajectories tend to a limit cycle located at $r = [-c(1 + \sqrt{1 - 4\alpha f/c^2})/2f]^{1/2}$, corresponding to the regular firing trajectory. If α is decreased such that $c^2/4f < \alpha < 0$, then $r = 0$ becomes a stable fixed point, and it coexists with a stable limit cycle at $r = [-c(1 + \sqrt{1 - 4\alpha f/c^2})/2f]^{1/2}$. The two attractors are separated by an unstable limit cycle located at $r = [-c(1 - \sqrt{1 - 4\alpha f})/2c^2]^{1/2}$. If α is decreased even further, such that $\alpha < c^2/4f$, a single stable manifold remains: a fixed point at $r = 0$, representing the subthreshold resting state.

The stable limit cycle of the firing trajectory has a minimal radius of $\sqrt{-c/2f}$, when $\alpha = c^2/4f$. Therefore, spike generation will be associated with the moment where the system crosses the border $\theta = \pi$ with a radius $r \geq \sqrt{-c/2f}$.

As before, the phase-resetting curves can be evaluated analytically (Brown et al., 2004),

$$Z(t) \propto \sin\left[2\pi(t - t_0)/T\right], \tag{2.6}$$

where t_0 and the proportionality constant can be evaluated in terms of the parameters of the original HH model. Figure 2D depicts the phase-response curve of equation 2.6. As observed in the full HH model, external perturbations may either advance or delay spiking, depending on when in the cycle they are delivered. By comparing the phase-response curves in Figures 2A and 2C and those in Figures 2B and 2D, we conclude that the qualitative features of the biophysically realistic models are captured by the reduced models.

In this work, we are interested in relating phenomenological description of the input-output mapping carried out by a given cell with the dynamical properties of the cell. In this context, it is interesting to point out that type I and type II neuron models have qualitatively different phase-response curves. This property suggests that the two neural types are selective to different stimulus features. This hypothesis was confirmed by Ermentrout, Galán, and Urban (2007), where they indicated that in quasi-periodically oscillating neurons that are weakly perturbed by input noise, the spike-triggered average is proportional to the derivative of the phase-response curve. Hence, when a neuron is stably circling around its firing limit cycle, the shape of the phase-response curve is highly informative of the stimulus features that induce spiking. In this letter, however, we are interested in analyzing the behavior of neuron models in the vicinity of firing onset. Therefore, the results derived in the suprathreshold regime are not necessarily applicable. In fact, Agüera y Arcas et al. (2003) have shown a spike-triggered average in HH neurons in the excitable regime that strongly resembles the phase-response curve itself (see Figure 2), and not its derivative. Both studies, hence, indicate that the phase-response curve contains information about the relevant stimulus features inducing spiking. The exact relationship between the two quantities, however, seems to depend critically on the mean level of depolarization. In this letter, we disclose the optimal stimulus features driving a cell that is initially near its resting state and that only occasionally generates action potentials. We therefore work with highly variable spike trains, as opposed to Ermentrout et al. (2007).

3 Covariance Analysis and the Extraction of Relevant Stimulus Features

In order to explore the stimuli that are most relevant in shaping the probability of spiking, we use spike-triggered covariance techniques (Bialek & de Ruyter von Steveninck, 2003; Paninski, 2003; Schwartz, Pillow, Rust, &

Simoncelli, 2006). Our purpose is to relate the results obtained from this standard statistical approach (which essentially treats the cell as a black box operating as an input-output device) with the internal (that is, dynamical) properties of the neurons.

If $P[\text{spike at } t_0|s(t)]$ is the probability of generating a spike at time t_0 conditional to a time-dependent stimulus $s(t)$, we assume that P depends on only the stimulus $s(t)$ through a few relevant features $f^1(t-t_0)$, $f^2(t-t_0), \ldots, f^k(t-t_0)$. The stimulus and the relevant features are continuous functions of time. For computational purposes, however, we represent them as vectors $\mathbf{s}$ and $\mathbf{f}^i$ of N components, where each component $s_j = s(j\delta t)$ and $f^i_j = f^i(j\delta t)$ is the value of the stimulus evaluated at discrete intervals δt. If δt is small compared with the relevant timescales of the models, this will be a good approximation.

The relevant features $\mathbf{f}^1, \ldots, \mathbf{f}^k$ lie in the space spanned by those eigenvectors of the matrix

$$M = C^{-1}_{\text{prior}} C_{\text{spikes}}, \tag{3.1}$$

whose eigenvalues are significantly different from unity (Schwartz et al., 2006). Here, C_{spikes} is the $N \times N$ spike-triggered covariance matrix,

$$(C_{\text{spikes}})_{ij} = \frac{1}{N_{\text{spikes}}} \sum_{t_0} s(t_i + t_0)s(t_j + t_0) - s^0(t_i)s^0(t_j), \tag{3.2}$$

where the sum is taken over all the spiking times t_0, and $s^0(t)$ is the spike-triggered average (STA):

$$s^0(t) = \frac{1}{N_{\text{spikes}}} \sum_{t_0} s(t + t_0). \tag{3.3}$$

Similarly, C_{prior} (also with dimension $N \times N$) is the prior covariance matrix,

$$(C_{\text{prior}})_{ij} = \overline{s(t_i + t)s(t_j + t)} - (\bar{s})^2, \tag{3.4}$$

where the horizontal line represents a temporal average on the variable t.

The eigenvalues of M that are larger than 1 are associated with directions in stimulus space where the stimulus segments associated with spike generation have an increased variance, as compared to the raw collection of stimulus segments. More precisely, the eigenvalue itself provides a measure of the ratio of variances of the two ensembles. Correspondingly, eigenvalues that lie significantly below unity are associated with stimulus directions of decreased variance. That is, an eigenvalue that is noticeably smaller than unity indicates a certain feature for which the ratio of the variance of the spike-triggering stimuli and the variance of the raw stimuli is significantly small.

In order to perform a covariance analysis of a specific neuronal model, we simulate the cell with an input current,

$$I(t) = I_0 + \sigma\xi(t). \tag{3.5}$$

The DC term I_0 lies slightly below threshold, so that the cell is not able to generate spikes in the absence of the gaussian noise term $\xi(t)$. The firing rate is regulated by adjusting σ. The noise $\xi(t)$ is such that $\langle\xi(t)\rangle = 0$ and $\langle\xi(t)\xi(t')\rangle = \tau \exp(-|t - t'|/\tau)/2$. In what follows, we use $\tau = 0.1$ or 0.2 ms, which is much faster than the characteristic time constants of the models and much slower than the numerical integration time 0.01 ms.

The input current given by equation 3.5 is injected into the realistic models (WB and HH) as an additive term in the equations governing the temporal evolution of the voltage variable (see equations A.1 and B.2, in the appendixes). For the type I model, η is proportional to the injected current $I(t)$ of equation 3.5. Hence, in equation 2.2, η is replaced by $I(t)$, with I_0 slightly below zero. Spike generation is identified with $\theta = \pi$. In the case of type II neurons, $I(t)$ should be parallel to the voltage variable. However, the two-dimensional system of equations 2.4 and 2.5 does not need to contain the voltage axis of the original HH system, since none of the two eigenvectors associated with the two eigenvalues that lose stability at threshold is necessarily parallel to the voltage axis. However, the voltage axis is not orthogonal to this two-dimensional system. Hence, if an input current drives the original HH system, that current has a nonzero projection onto the reduced two-dimensional system. The reduced system should therefore be excited in the direction in which the original voltage axis projects onto the subspace spanned by the eigenvectors associated with the two eigenvalues that lose stability. In our simulations, the input current, equation 3.5, was injected, making a 45 degree angle with the x-axis. We have verified, however, that our results do not depend critically on the value of this angle.

4 Relevant Stimulus Features Driving Type I Neurons

The results of a covariance analysis of the WB model are depicted in Figure 3. In Figure 3A, the spectrum of eigenvalues of a 10 Hz firing neuron is shown. The majority of the eigenvalues cluster around unity. There is, however, a single eigenvalue that is notoriously smaller than all the others. This spectrum remains essentially unchanged, as the firing rate of the neuron is varied between 2.5 and 40 Hz. In Figure 3B, the eigenvector corresponding to the smallest eigenvalue shown in Figure 3A is depicted by a dotted line. The other lines show how this eigenvector changes as the firing rate of the cell is modified. This is accomplished by fixing the noise σ to different values. Hence, the different curves in Figure 3B correspond to the single relevant eigenvector obtained for different firing rates (see the line conventions in Figure 3C).

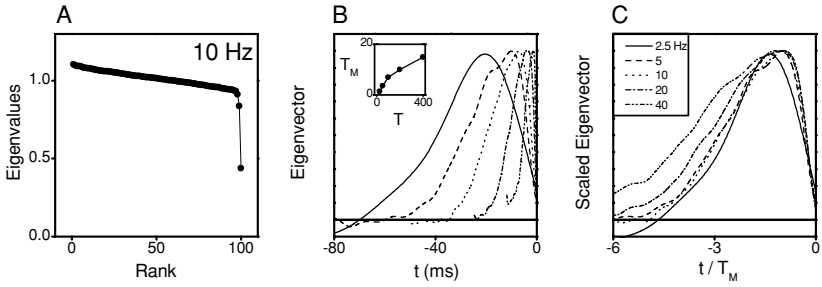

Figure 3: Covariance analysis of the WB model. In all cases, $I_0 = 0$, $\tau = 0.2$ ms. (A) Eigenvalue spectrum obtained for 10 Hz ($\sigma = 15.5\ \mu\text{A/cm}^2\text{ms}^{1/2}$, CV = 0.74, 50,420 spikes). The qualitative aspect of the spectrum of eigenvalues remains the same for all firing rates shown in *B* and *C*. (B) Eigenvectors corresponding to the smallest eigenvalue. Different curves are obtained by setting the noise σ to different values, and thereby, by varying the firing rate: 2.5 Hz ($\sigma = 8.1\ \mu\text{A/cm}^2\text{ms}^{1/2}$, CV = 0.87; 55,099 spikes), 5 Hz ($\sigma = 10.3\ \mu\text{A/cm}^2\text{ms}^{1/2}$, CV = 0.81; 50,956 spikes), 10 Hz ($\sigma = 15.5\ \mu\text{A/cm}^2\text{ms}^{1/2}$, CV = 0.87; 55,099 spikes), 20 Hz ($\sigma = 25.5\ \mu\text{A/cm}^2\text{ms}^{1/2}$, CV = 0.74; 50,790 spikes), 40 Hz ($\sigma = 69.0\ \mu\text{A/cm}^2\text{ms}^{1/2}$, CV = 0.81; 49,110 spikes). As the firing rate grows, the eigenvector becomes increasingly narrow. Line conventions shown in *C*. Inset: Time T_M at which each eigenvector reaches its maximum value as a function of the mean interspike interval T (the inverse of the firing rate). (C) Scaled eigenvectors for different firing rates. Hence, at firing onset, the WB model is sensitive to a universal depolarizing stimulus whose temporal scale depends solely on the firing rate of the cell.

For all firing rates, we see that there is a single eigenvalue that is significantly smaller than unity. This means that the relevant eigenvector corresponds to a stimulus direction with diminished variance. In all cases, the relevant eigenvector shows a unimodal curve that is either always positive or always negative (recall that the sign of an eigenvector is not determined by the covariance analysis). In Figure 3 we have chosen to represent the eigenvectors as positive (and not negative) stimulus segments, because in this way, they coincide with the STA (data not shown). This allows us to conclude that the WB neuron model fires in response to depolarizing stimuli. This result is in agreement with the phase-resetting curves obtained for the WB model (see Figure 2A). Hence, although phase-resetting curves (necessarily calculated with stimuli of supra-threshold mean) and our covariance analysis (carried out with stimuli of subthreshold mean) correspond to two different firing regimes, there is a qualitative parallelism between them: in type I neurons near their firing onset, depolarizing input currents always favor spike generation.

In Figure 3B we see that as the firing rate increases, the relevant stimulus feature reduces the span of its temporal domain. By naked eye, it seems

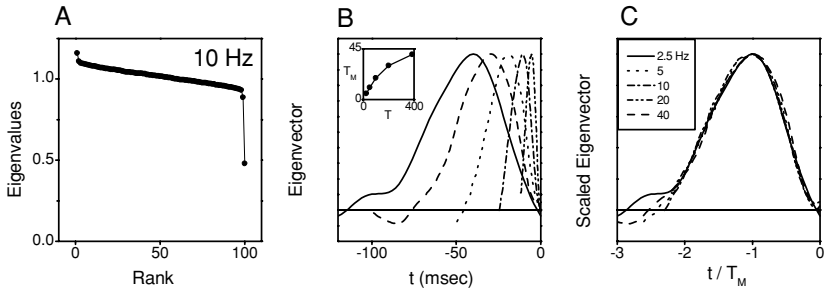

Figure 4: Covariance analysis of the normal form of type I neurons. Spike generation is identified as θ crossing the angle π. In all cases, $I_{DC} = -0.01\mu A/cm^2$, and $\tau = 0.2$ ms. (A) Eigenvalue spectrum obtained for 10 Hz ($\sigma = 0.0046$ $\mu A/cm^2 ms^{1/2}$, CV = 0.64; 50,607 spikes). (B) Eigenvectors corresponding to the smallest eigenvalue. Different curves correspond to different firing rates: 2.5 Hz ($\sigma = 0.002935$ $\mu A/cm^2 ms^{1/2}$, CV = 0.81; 51,718 spikes), 5 Hz ($\sigma = 0.00353$ $\mu A/cm^2 ms^{1/2}$, CV = 0.73; 49,855 spikes), 10 Hz ($\sigma = 0.0046$ $\mu A/cm^2 ms^{1/2}$, CV = 0.64; 50,607 spikes), 20 Hz ($\sigma = 0.00715$ $\mu A/cm^2 ms^{1/2}$, CV = 0.60; 49,962 spikes), 40 Hz ($\sigma = 0.01421$ $\mu A/cm^2 ms^{1/2}$, CV = 0.57; 50,296 spikes). Inset: Time T_M at which each eigenvector reaches its maximum value as a function of the mean interspike interval T (the inverse of the firing rate). (C) Scaled eigenvectors for different firing rates. The normal type I model, hence, shows the same qualitative behavior as the conductance-based WB model.

that the main effect of changing the firing rate is a temporal rescaling of the eigenvector. In order to check this hypothesis, for each firing rate we determine the time T_M at which the relevant eigenvector reaches its peak value. In the inset of Figure 3B, T_M is depicted as a function of the mean interspike interval T (the inverse of the firing rate). Next, we rescale each eigenvector by plotting it as a function of t/T_M, as shown in Figure 3C. There we see that throughout a 16-fold increase in the firing rate, the shape of the relevant eigenvector remains essentially unchanged, apart from a temporal scaling. This implies that near threshold, spike generation in the WB model is governed by a single relevant stimulus feature of universal shape.

How general is this universality? Following Ermentrout and Kopell (1986) and Ermentrout (1996), in the previous section we pointed out that as an arbitrary type I neuron approaches threshold, its dynamical equations can be reduced to the normal form, equation 2.2. Recall that the single parameter appearing in equation 2.2 is proportional to the (scaled) perturbative input current i. Though this reduction is valid only under constant stimulation, the absence of typical timescales in the normal form of type I neurons suggests that perhaps the universal eigenvector shown in Figure 3 might be a general property of type I models near firing onset. In order to check this hypothesis, in Figure 4 we depict the results of performing a

covariance analysis of the normal-form dynamical model of equation 2.2. In Figure 4A, the eigenvalue spectrum obtained for 10 Hz firing rate is shown. As in the WB model, the most salient eigenvalue is significantly smaller than unity. The largest eigenvalue also seems to depart from unity. We have checked, however, that as one gets closer to threshold (as $I_{DC} \to 0^-$), this eigenvalue approaches unity.

Just as it happened with the WB model, near threshold, the spectrum of eigenvalues remains essentially unchanged, as the firing rate is varied: in all cases, there is a single eigenvalue significantly smaller than unity. In Figure 4B, the eigenvector corresponding to this eigenvalue is depicted, for different values of the firing rate. The same qualitative behavior seen in Figure 3 is obtained: as the firing rate grows, the depolarizing fluctuation in the eigenvector becomes increasingly time compressed. In the inset of Figure 4B, we show the time T_M at which the eigenvector reaches its maximum value as a function of the mean period T (the inverse of the mean firing rate). In Figure 4C, the scaled eigenvectors may be seen to fit a fairly universal shape in spite of the 16-fold variation in the firing rates. Hence, we conclude that the universal behavior observed in the WB model is actually a general property of type I neurons, near threshold.

5 Relevant Stimulus Features Driving Type II Neurons

In the previous section we saw that type I neurons fire in response to depolarizing stimulus fluctuations and that those fluctuations lack an intrinsic temporal scale: the faster the stimulus, the higher the firing rate. Here, we explore whether that is also the case for type II neurons. In Figure 5 we show the results of carrying out a covariance analysis with the HH model neuron, for two values of the firing rate: 10 Hz (upper panels) and 20 Hz (lower panels). Each spectrum of eigenvalues (see Figures 5A and 5D) exhibits two outliers, labeled *a* and *b* in the figure. The corresponding eigenvectors are depicted in Figures 5B and 5E (in the time domain) and in Figures 5C and 5F (in the frequency domain). In all cases, the eigenvectors exhibit both positive and negative phases. This result is in agreement with the phase-resetting curves obtained for the suprathreshold HH model (see Figure 2B), suggesting that the relevant subspace comprises characteristic frequencies. For both firing rates, we observe that each eigenvector contains a dominant frequency: eigenvector *a* peaks at 125 Hz, whereas *b* reaches its maximum at 62 Hz. As may be easily judged by comparing Figures 5B and 5E, the temporal domain of the eigenvectors does not seem to contract, as the firing rate is doubled. Accordingly, the principal frequency of each eigenvector (compare Figures 5C and 5F) remains unaltered. This means that in the HH model, each eigenvector has a characteristic temporal pattern that is not determined by the firing rate of the cell. A natural question, hence, arises: What governs these temporal patterns and their characteristic frequencies?

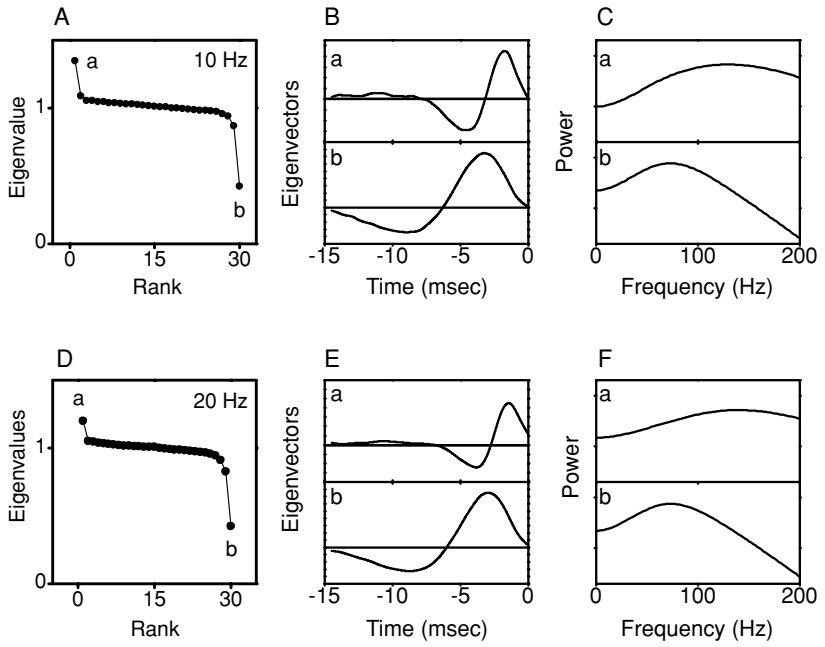

Figure 5: Covariance analysis of the HH model neuron for two values of the firing rate, for $\tau = 0.2$; ms. (Upper panels) 10 Hz firing rate ($\sigma = 17.2\mu\text{A/cm}^2\,\text{ms}^{1/2}$, CV $= 0.85$; 51,165 spikes). (Lower panels) 20 Hz firing rate ($\sigma = 22.15\mu\text{A/cm}^2\,\text{ms}^{1/2}$, CV $= 0.69$; 51,490 spikes). (A, D) Spectra of eigenvalues. In each case, two outliers are singled out, labeled as a and b. (B, E) Time domain representation of the eigenvectors corresponding to the eigenvalues a and b. (C, F) Frequency domain representation of the eigenvectors a and b.

To answer this question, we apply covariance-analysis techniques to the reduced model described by equations 2.4 and 2.5. In the first place, we choose $c = 1/\text{ms}$ and $f = -1/\text{ms}$. Moreover, we fix $\dot{\theta} = \text{cnst} = 2\pi\beta$ (that is, we make $g = d = 0$). This means that the whole reduced system, equations 2.4 and 2.5, revolves with a unique angular velocity β around the origin. In Figure 6, the results obtained for two different values of β are shown. In the upper panels, $\beta = 1/\text{ms}$, in the lower ones, $\beta = 1/2$ ms. In Figures 6A and 6E, the dependence of $\dot{\theta}$ with the radial variable r is shown. In Figures 6B and 6F, we see the spectra of eigenvalues. In both cases, two almost degenerate eigenvalues (labeled a and b) are significantly smaller than unity. The eigenvectors corresponding to these two eigenvalues are shown in Figures 6C and 6G. For each value of β, the eigenvectors a and b are very similar to each other: they constitute an almost sinusoidal waveform of a very well-defined frequency. They differ only in a $\pi/2$ phase shift,

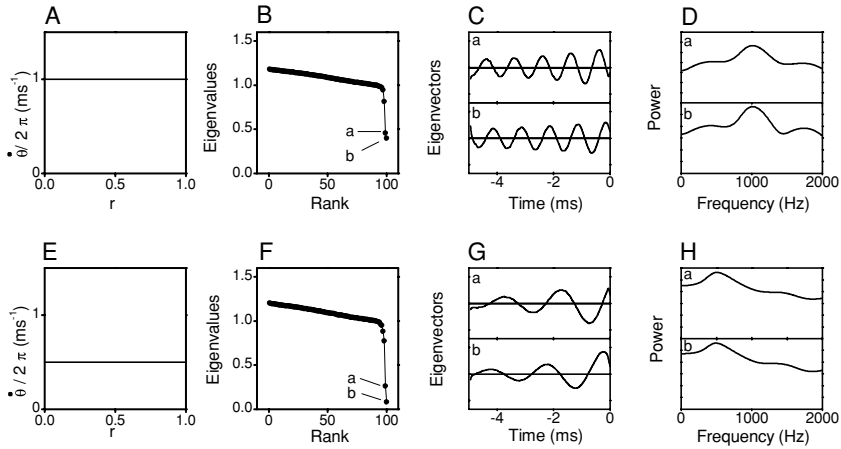

Figure 6: Covariance analysis of a normal form type II neuron model in which the angular velocity $\dot{\theta}$ is independent of the radial coordinate. The bifurcation parameter α is set to -0.5/ms, and $\tau = 0.1$ ms. The noise σ is chosen so as to obtain a firing rate of 200 Hz. (Upper panels) $\beta = 1$/ms, $\sigma = 0.037/\text{ms}^{1/2}$, CV $= 2.3$; 48,246 spikes. (Lower panels) $\beta = 0.5$ ms, $\sigma = 0.0798/\text{ms}^{1/2}$, CV $=$ 1.3; 49,923 spikes. (A, E) Dependence of the angular velocity $\dot{\theta}$ on the radial coordinate r. (B, F) Spectra of eigenvalues. Two almost degenerate outliers are clearly seen. (C, G) Eigenvectors in the temporal domain. (D, H) Eigenvectors in the frequency domain, plotted in logarithmic scale.

implying that the relevant stimulus eigenspace comprises all linear combinations of a sine and a cosine function, of a specific frequency. The frequency, though, varies with β. Figures 6D and 6H show the power spectra of the two eigenvectors in logarithmic scale. When $\beta = 1$/ms, the maximum power is found at a frequency of 1000 Hz (see Figure 5D), whereas for $\beta = 0.5$/ms, the eigenvectors peak at 500 Hz (see Figure 5H). This means that we are in the presence of a resonance phenomenon: spiking probability is maximized shortly after stimulus segments that contain significant power in the characteristic frequency of the angular motion of the dynamical system.

How do these results change when the angular velocity $\dot{\theta}$ depends on the radial coordinate r? This question is pertinent, since type II systems undergo two bifurcations, in two different locations in phase space, and are therefore not amenable of a local reduction. The firing limit cycle appears through a global bifurcation that in principle may take place far away from the resting fixed point. Hence, the frequency associated with the spiking limit cycle need not coincide with the frequency of subthreshold oscillations. Therefore, in Figure 7 we explore the behavior of two other type II systems, where the angular velocity $\dot{\theta}$ either increases with r (upper panels) or decreases with r (lower panels). We see that once the angular velocity

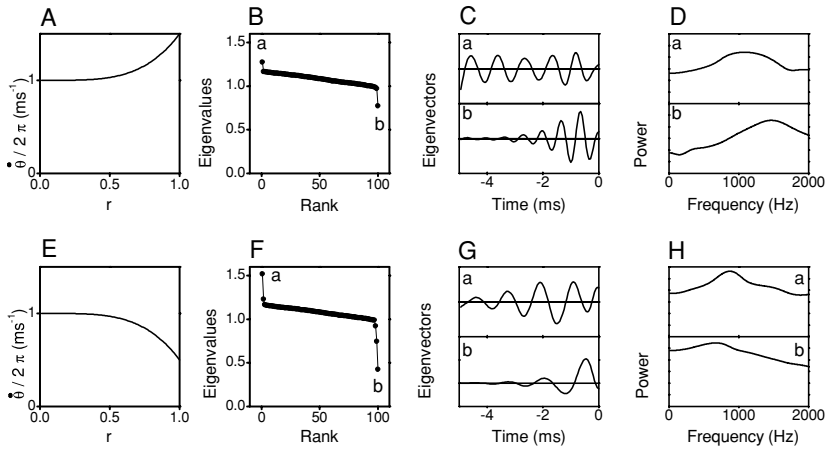

Figure 7: Covariance analysis of a normal-form type II neuron model in which the angular velocity $\dot{\theta}$ either increases with the radial coordinate r (upper panels) or decreases with r (lower panels). The bifurcation parameter α is set to $-0.5/\text{ms}$, and $\tau = 0.1$ ms. The noise σ is chosen so as to obtain a firing rate of 200 Hz. (Upper panels): $\beta = 1/\text{ms}$, $g = 0.5$, $\tau = 0.1$ ms, $\sigma = 0.025/\text{ms}^{1/2}$, CV = 6.0; 234,796 spikes. (Lower panels) $\beta = 0.5\,\text{ms}$, $g = -0.5$, $\tau = 0.1$ ms, σ=0.025 $0.049/\text{ms}^{1/2}$, CV = 1.3; 200,212 spikes. (A, E) Dependence of the angular velocity $\dot{\theta}$ on the radial coordinate r. (B, F) Spectra of eigenvalues. Two outliers are clearly seen, one of them (a) with increased variance, the other one (b) with decreased variance. (C, G) Eigenvectors in the temporal domain. (D, H) Eigenvectors in the frequency domain, plotted in logarithmic scale.

$\dot{\theta}$ sweeps over a whole range of frequencies, the degeneracy of the relevant eigenvectors is removed. Actually, now one of the eigenvectors (*a*) is associated with a direction of increased variance, and the other one (*b*) corresponds to a diminished variance. Eigenvector b is still centered around the frequency of subthreshold oscillations near the fixed point (that is, 1000 Hz). However, the dominant frequency of eigenvector b has now shifted to a lower or higher value, depending on whether $\dot{\theta}$ is an increasing or decreasing function of r. In the upper panels, $\dot{\theta}$ grows with r, implying that the firing limit cycle has a higher frequency than the subthreshold oscillations. Correspondingly, the dominant frequency of eigenvector b is shifted to higher values (see Figure 7D). The lower panels instead show a case in which $\dot{\theta}$ is a decreasing function of r, and correspondingly, the dominant frequency of eigenvector b has shifted to lower values (see Figure 7H).

In an arbitrary type II system, the angular velocity may show a rather complicated dependence on the radial coordinate r. In consequence, the prototypical system described by equations 2.4 and 2.5 contains several nontrivial parameters. The shape of the spectrum of eigenvalues depends

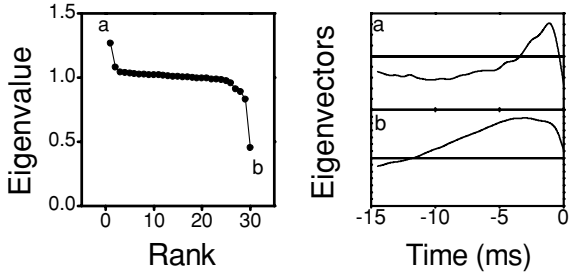

Figure 8: Covariance analysis of a normal-form type II neuron model in which the parameters have been chosen in order to obtain two eigenvectors that span a subspace that is qualitatively similar to the one generated by the eigenvectors of the HH model (see Figure 5). Here, $\tau = 0.2$ ms, $c = 1.69/\text{ms}$, $f = -1.69/\text{ms}$, $\beta = 0.0477/\text{ms}$, $d = -0.0183/\text{ms}$, $g = 0$, $\alpha = -0.3/\text{ms}$, $\sigma = 0.028/\text{ms}^{1/2}$, CV $=$ 0.79; 49,409 spikes. The firing rate was 21.0 Hz.

rather critically on these parameters, and so do the associated eigenvectors. Actually, by choosing those parameters carefully, it is possible to obtain eigenvalues and eigenvectors that are similar to those of the original HH model. In Figure 8, we show the results of stimulating the normal form, equations 2.4 and 2.5, with conveniently selected values of the parameters $\alpha, c, f, \beta, d, g$ so as to obtain an eigenspace that is qualitatively similar to the one generated by the eigenvectors of the HH model of Figure 5. Notice that with these parameters, $\mathrm{d}\theta/\mathrm{d}t$ is a decreasing function of r. This is in agreement with the behavior of the HH model, where the frequency associated with the firing limit cycle is smaller than the frequency of the subthreshold oscillations around the resting state.

6 Discussion

In this letter, we have analyzed the stimulus features that are relevant in shaping the spiking probability for type I and type II neuron models. Type I models undergo a saddle node, away-limit-cycle bifurcation at firing onset, and they can be reduced to a normal form that contains a single scale parameter that determines the firing frequency. Our analysis shows that when type I models are stimulated with random input currents whose mean value lies slightly below threshold, they fire in response to depolarizing stimuli. By scaling the relevant eigenvectors obtained from a covariance analysis, we have shown that type I models are not selective to specific temporal scales: the faster the depolarizing input, the faster the neural response.

Previous studies (Agüera y Arcas & Fairhall, 2003) have shown that the firing probability of integrate-and-fire neurons is determined by a

two-dimensional space, spanned by the eigenvectors associated with small-variance and large-variance eigenvalues. The eigenvector associated with the small eigenvalue essentially coincided with the eigenvector shown in the type I models in section 4. The second eigenvector obtained for the integrate-and-fire model, however, combines a hyperpolarizing and a depolarizing phase. In the models studied in section 4, that eigenvector could sometimes be identified (see the largest eigenvalue of Figure 4). However, as the DC component of the input current approaches the threshold current, the eigenvalue was shown to decrease, until it was hidden in the baseline level of all the other eigenvalues (see Figure 3). This effect, however, is not found in the integrate-and-fire model, for which all input currents are represented by a spectrum of eigenvalues showing two outliers. Hence, integrate-and-fire neurons do not behave as our prototypical type I neurons. The reason for this discrepancy lies in the fact that near threshold, the slow evolution of integrate-and-fire neurons revolves around the zone of phase space representing the firing threshold. In the type I neuron models discussed in this letter, slow dynamics occurs in the vicinity of the subthreshold resting state. Hence, the two models cannot be mapped onto one another without the introduction of additional abrupt dynamical features, as the voltage cutoffs employed in Hansel and Mato (2003).

In contrast, type II models are governed by a subcritical Hopf bifurcation, thereby requiring a two-dimensional, nonlocal description. As a consequence, type II models are characterized by several parameters that retain various temporal properties of the original dynamical system. These differences between type I and type II neuron models imply that each one of them is responsive to particular features of the input current. Baroni and Varona (2007) have suggested that the differences in the input-output transformation carried out by type I and type II neurons may have evolved to activate different populations of neurons, depending on the specific temporal patterns of the presynaptic input. Muresan and Savin (2007), in turn, have discussed the consequences of these differences at the network level. While type II neurons favor self-sustainability of network activity, type I cells increase the richness of the responsiveness to external stimuli.

The main distinction between the stimulus features driving type I and type II models, as demonstrated by our covariance analysis, provides further justification to the distinction introduced by Izhikevich (2001), where type I neurons are called *integrators* and Hopf-like type II neurons are *resonators*. Our work shows that near threshold, type I neurons are essentially waiting to receive excitatory input (no matter their timescale), whereas Hopf-like type II neurons are able to detect input segments that contain sufficient power in the frequency band that is well represented by their intrinsic dynamics.

Can the relevant stimulus features be connected to the phase-resetting curves? By comparing Figure 2 with Figure 3, we conclude that both the

phase-response curve and the preferred stimulus features of type I neurons (which, as stated above, coincide with the STA) are monophasic and positive. In turn, both the eigenvector corresponding to the smallest eigenvalue of type II neurons (the one that is most similar to the STA) and the phase-response curve exhibit positive and negative phases (compare Figures 2 and 5). This similarity, however, can be stated only at a qualitative level. Recall that phase-response curves can be defined only in the suprathreshold regime, whereas the covariance analysis concerned random input currents of subthreshold mean.

Ermentrout et al. (2007) have proved that when a cell is firing regularly while receiving mild random perturbative currents, its spike-triggered average is equal to the temporal derivative of the phase-resetting curve. This result contrasts with our observation that the phase-response curve itself (and not its derivative) has the same sign as the relevant stimulus features inducing spiking, for subthreshold stimuli. The two conclusions, however, are not in conflict with one another. In Figure 9, the ISI distribution, the STA, and the most relevant eigenvector of a normal form, type I neuron are shown, when driven with three different stimulation protocols. The plots on the left correspond to an input stimuli whose mean value is sufficiently large as to keep the system firing regularly at 20 Hz. The noisy component of the injected current therefore only rarely modifies the regular spiking pattern, occasionally advancing or delaying an action potential. As a consequence, the interspike interval (ISI) distribution reduces to a very narrow peak located at 50 ms. The STA, in turn, is clearly biphasic and constitutes a very good approximation of the temporal derivative of the phase-resetting curve (see Ermentrout et al., 2007). The most relevant eigenvector is qualitatively similar to the STA, though its shape is noticeably more sensitive to limited sampling.

In order to explore how these results evolve as the activity of the cell becomes more irregular, in the middle and right panels we show the results obtained with other stimulating scheme, where the mean stimulus is lowered and the stochastic component of the input current is increased as to maintain a 20 Hz firing rate. The ISI distributions are therefore significantly widened. We see that the STA is no longer symmetric with respect to the mean stimulus: the depolarized phase of the STA is markedly larger than the hyperpolarized one. As the mean stimulus is made increasingly negative, the negative phase disappears completely, and the STA merges into the curves shown in Figure 4. We therefore conclude that the exact relationship between the relevant stimulus features inducing spiking and the phase-response curve depends critically on how regular the spike train is, which, for fixed firing rate, is governed by the ratio between the SD of the stimulus and its mean value. We hope that this analysis may serve to inspire future investigations in the connection between these quantities.

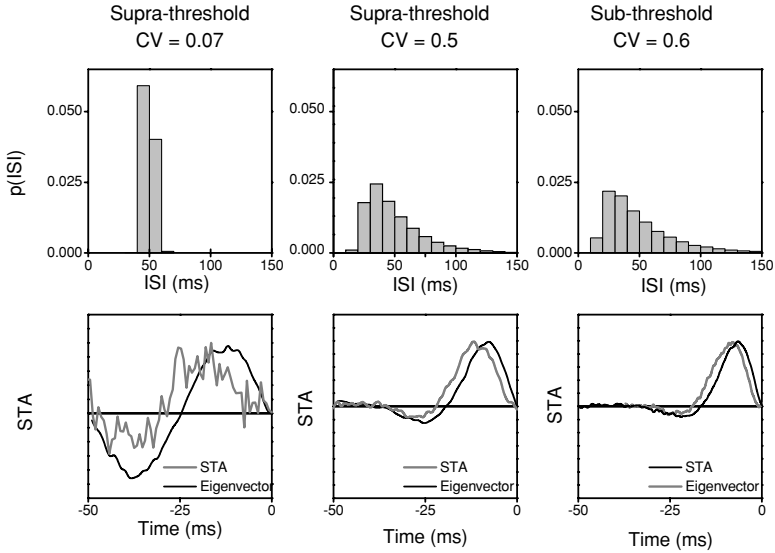

Figure 9: ISI probability densities (upper panels) and most relevant stimulus feature (lower panels) of a normal-form, type I neuron firing at 20 Hz for three different stimulation protocols. The most relevant stimulus feature is obtained with two different methods: the STA (black line) and the most prominent eigenvector (gray line). (Left) Regular firing, with stimuli of suprathreshold mean. $\alpha = 0.004$, $\sigma = 0.00029$ ms$^{1/2}$, $\tau = 0.2$ ms; 500,159 spikes, CV $= 0.07$. (Middle) Irregular firing, with stimuli of small suprathreshold mean. $\alpha = 0.002$, $\sigma = 0.00295$ ms$^{1/2}$, $\tau = 0.2$ ms; 201,287 spikes, CV $= 0.5$. (Right) Irregular firing, with stimuli of small subthreshold mean. $\alpha = -0.001$, $\sigma = 0.004345$ ms$^{1/2}$, $\tau = 0.2$ ms; 49,462 spikes, CV $= 0.6$. When the system is firing regularly (low CV), the STA shows a positive and a negative phase, resembling the derivative of the phase-resetting curve. In contrast, when the system fires in an irregular fashion (large CV), the STA exhibits a large positive phase and a small negative portion.

Appendix A: Wang Buzsaki (WB) Model

The dynamical equations for the conductance-based type I neuron model used in this work were introduced by Wang and Buzsaki (1996):

$$C\frac{\mathrm{d}V}{\mathrm{d}t} = I - g_{\mathrm{Na}}\mathrm{m}_{\infty}^{3}(V)h(V-V_{\mathrm{Na}}) - g_{\mathrm{K}}n^{4}(V-V_{\mathrm{K}}) - g_{\ell}(V-V_{\ell}) \quad \text{(A.1)}$$

$$\frac{\mathrm{d}h}{\mathrm{d}t} = \frac{\mathrm{h}_{\infty}(V)-h}{\tau_{\mathrm{h}}(V)} \quad \text{(A.2)}$$

$$\frac{dn}{dt} = \frac{\mathrm{n}_{\infty}(V)-n}{\tau_{\mathrm{n}}(V)}. \quad \text{(A.3)}$$

The parameters g_{Na}, g_{K}, and g_ℓ are the maximum conductances per surface unit for the sodium, potassium, and leak currents, respectively, and V_{Na}, V_{K}, and V_ℓ are the corresponding reversal potentials. The capacitance per surface unit is denoted by C. The external stimulus on the neuron is represented by an external current I. The functions $\mathrm{m}_\infty(V)$, $\mathrm{h}_\infty(V)$, and $\mathrm{n}_\infty(V)$ are defined as $\mathrm{x}_\infty(V) = a_{\mathrm{x}}(V)/[a_{\mathrm{x}}(V) + b_{\mathrm{x}}(V)]$, where x = m, n, or h. In turn, the characteristic times (in milliseconds) τ_{n} and τ_{h} are given by $\tau_{\mathrm{x}} = 1/[a_{\mathrm{x}}(V) + b_{\mathrm{x}}(V)]$, and

$$a_{\mathrm{m}} = -0.1(V + 35)/(\exp(-0.1(V + 35)) - 1), \tag{A.4}$$

$$b_{\mathrm{m}} = 4\exp(-(V + 60)/18), \tag{A.5}$$

$$a_{\mathrm{h}} = \phi\, 0.07\exp(-(V + 58)/20), \tag{A.6}$$

$$b_{\mathrm{h}} = \phi/(\exp(-0.1(V + 28)) + 1). \tag{A.7}$$

The delayed rectifier current is described in a similar way as in the HH model, with

$$a_n = \phi\, 0.01(V + 34)/(1 - \exp(-0.1(V + 34))), \tag{A.8}$$

$$b_n = \phi\, 0.125\exp(-(V + 44)/80). \tag{A.9}$$

Other parameters of the model are $V_{\mathrm{K}} = -90\,\mathrm{mV}$, $V_{\mathrm{Na}} = 55\,\mathrm{mV}$, $V_\ell = -65\,\mathrm{mV}$, $C = 1\,\mu\mathrm{F/cm^2}$, $g_\ell = 0.1\,\mathrm{mS/cm^2}$, $g_{\mathrm{Na}} = 35\,\mathrm{mS/cm^2}$, $g_{\mathrm{K}} = 9\ \mathrm{mS/cm^2}$, and $\phi = 3$.

Appendix B: The Hodgkin-Huxley Model

The dynamical equations of the Hodgkin-Huxley (Hodgkin & Huxley, 1952) model read

$$C\frac{\mathrm{d}V}{\mathrm{d}t} = I - g_{\mathrm{Na}}m^3h(V - V_{\mathrm{Na}}) - g_{\mathrm{K}}n^4(V - V_{\mathrm{K}}) - g_\ell(V - V_\ell), \tag{B.1}$$

$$\frac{\mathrm{d}m}{\mathrm{d}t} = \frac{\mathrm{m}_\infty(V) - m}{\tau_{\mathrm{m}}(V)}, \tag{B.2}$$

$$\frac{\mathrm{d}h}{\mathrm{d}t} = \frac{\mathrm{h}_\infty(V) - h}{\tau_{\mathrm{h}}(V)}, \tag{B.3}$$

$$\frac{\mathrm{d}n}{\mathrm{d}t} = \frac{\mathrm{n}_\infty(V) - n}{\tau_{\mathrm{n}}(V)}. \tag{B.4}$$

For the squid giant axon, the parameters at 6.3°C are $V_{\mathrm{Na}} = 50\,\mathrm{mV}$, $V_{\mathrm{K}} = -77\,\mathrm{mV}$, $V_\ell = -54.4\,\mathrm{mV}$, $g_{\mathrm{Na}} = 120\,\mathrm{mS/cm^2}$, $g_{\mathrm{K}} = 36\,\mathrm{mS/cm^2}$,

$g_\ell = 0.3\,\mathrm{mS/cm^2}$, and $C = 1\,\mu\mathrm{F/cm^2}$. The functions $\mathrm{m}_\infty(V)$, $\mathrm{h}_\infty(V)$, $\mathrm{n}_\infty(V)$, $\tau_\mathrm{m}(V)$, $\tau_\mathrm{n}(V)$, and $\tau_\mathrm{h}(V)$ are defined in terms of the functions $a(V)$ and $b(V)$ as in the WB model, but now

$$a_\mathrm{m} = 0.1(V + 40)/(1 - \exp((-V - 40)/10)), \tag{B.5}$$

$$b_\mathrm{m} = 4\exp((-V - 65)/18), \tag{B.6}$$

$$a_\mathrm{h} = 0.07\exp((-V - 65)/20)), \tag{B.7}$$

$$b_\mathrm{h} = 1/(1 + \exp((-V - 35)/10), \tag{B.8}$$

$$a_\mathrm{n} = 0.01(V + 55)/(1 - \exp((-V - 55)/10)), \tag{B.9}$$

$$b_\mathrm{n} = 0.125\exp((-V - 65)/80). \tag{B.10}$$

Acknowledgments

We thank Eugenio Urdapilleta for useful discussions. This work has been supported by the Consejo Nacional de Investigaciones Científicas y Técnicas (PIP 5140), the Alexander von Humboldt Foundation, the Universidad Nacional de Cuyo, and the Agencia Nacional de Promoción Científica y Tecnológica.

References

Agüera y Arcas, B., & Fairhall, A. L. (2003). What causes a neuron to spike? *Neural Comput., 15*, 1789–1807.

Agüera y Arcas, B., Fairhall, A. L., & Bialek, W. (2003). Computation in a single neuron: Hodgkin and Huxley revisited. *Neural Comput., 15*, 1715–1749.

Baroni, F., & Varona, P. (2007). Subthreshold oscillations and neuronal input-output relationships. *Neurocomput., 70*, 1611–1614.

Bialek, W., & de Ruyter von Steveninck, R. R. (2003). *Features and dimensions: Motion estimation in fly vision*. Unpublished manuscript.

Brown, E., Moehlis, J., & Holmes, P. (2004). On the phase reduction and response dynamics of neural oscillator populations. *Neural Comput., 16*, 673–715.

Ermentrout, B. (1996). Type I membranes, phase resetting curves, and synchrony. *Neural Comp., 8*, 979–1001.

Ermentrout, B., Galán, R., & Urban, N. (2007). Relating neural dynamics to neural coding. *Phys. Rev. Lett., 99*, 248103, 1–4.

Ermentrout, B., & Kopell, N. (1986). Parabolic bursting in an excitable system coupled with a slow oscillation. *SIAM Journal on Applied Mathematics, 46*, 233–253.

Fairhall, A., Burlingame, C. A., Narasimhan, R., Harris, R. A., Puchalla, J. L., & Berry, M. J. (2006). Selectivity for multiple stimulus features in retinal ganglion cells. *J. Neurophysiol., 96*, 2724–2738.

Hansel, D., & Mato, G. (2003). Asynchronous states and the emergence of synchrony in large networks of interacting excitatory and inhibitory neurons. *Neural Comput., 15*, 1–56.

Hansel, D., Mato, G., & Meunier, C. (1995). Synchrony in excitatory neural networks. *Neural Comput., 7*, 307–337.

Hodgkin, A. L. (1948). The local electric charges associated with repetitive action in non-medulated axons. *J. Physiol., 107*, 165–181.

Hodgkin, A. L., & Huxley, A. F. (1952). A quantitative description of membrane current and application to conductance in excitation nerve. *J. Physiol. (London), 117*, 500–544.

Hong, S., Agüera y Arcas, B., & Fairhall, A. (2007). Single neuron computation: From dynamical system to feature detector. *Neural Computation, 19*, 3133–3172.

Izhikevich, E. (2001). Resonate and fire neurons. *Neural Networks, 14*, 833–894.

Izhikevich, E. (2007). *Dynamical systems in neuroscience: The geometry of excitability and bursting*. Cambridge, MA: MIT Press.

Kuramoto, Y. (2003). *Chemical oscillations, waves and turbulence.* New York: Dover.

Maravall, M., Petersen, R. S., Fairhall, A. L., Arabzadeh, E., & Diamond, M. E. (2007). Shifts in coding properties and maintenance of information transmission during adaptation in barrel cortex. *PLoS Biol., 5*(2), e19.

Muresan, R. C., & Savin, C. (2007). Resonance or integration? Self-sustained dynamics and excitability of neural microcircuits. *J. Neurophysiol., 97*, 1911–1930.

Paninski, L. (2003). Convergence properties of some spike-triggered analysis techniques. *Network, 14*, 437–464.

Rust, N. C., Schwartz, O., Movshon, J. A., & Simoncelli, E. P. (2005). Spatiotemporal elements of macaque V1 receptive fields. *Neuron., 46*, 945–956.

Schwartz, O., Pillow, J. W., Rust, N. C., & Simoncelli, E. P. (2006). Spike-triggered neural characterization. *J. Vision, 6*, 484–507.

Wang, X. J., & Buzsáki, G. (1996). Gamma oscillation by synaptic inhibition in a hippocampal interneuronal network model. *J. Neurosci., 16*, 6402–6413.

Received October 29, 2007; accepted January 11, 2008.